

AKARI observations of circumstellar dust in the globular clusters NGC104 and NGC362

Yoshifusa ITA

¹*Institute of Space and Astronautical Science, Japan Aerospace Exploration Agency
3-1-1 Yoshinodai, Sagami-hara, Kanagawa 229-8510, Japan
yita@ir.isas.jaxa.jp*

Toshihiko TANABÉ², Noriyuki MATSUNAGA², Yoshikazu NAKADA², Mikako MATSUURA³,
²*Institute of Astronomy, Graduate School of Science,*

The University of Tokyo, 2-21-1 Osawa, Mitaka, Tokyo 181-0015, Japan

³*National Astronomical Observatory of Japan, 2-21-1 Osawa, Mitaka, Tokyo, 181-8588, Japan
and*

Takashi ONAKA⁴, Hideo MATSUHARA¹, Takehiko WADA¹, Naofumi FUJISHIRO⁵, Daisuke ISHIHARA⁴,
Hirokazu KATAZA¹, Woojung KIM¹, Toshio MATSUMOTO¹, Hiroshi MURAKAMI¹, Youichi OHYAMA¹,
Fumihiko USUI¹, Shinki OYABU¹, Itsuki SAKON⁴, Toshinobu TAKAGI¹, Kazunori UEMIZU¹,
Munetaka UENO⁶, Hidenori WATARAI⁷

⁴*Department of Astronomy, Graduate School of Science,
The University of Tokyo, Bunkyo-ku, Tokyo 113-0033, Japan*

⁵*Department of Physics, Graduate School of Science,
The University of Tokyo, Bunkyo-ku, Tokyo 113-0033, Japan*

⁶*Department of Earth Science and Astronomy, Graduate School of Arts and Sciences,
The University of Tokyo, Meguro-ku, Tokyo 153-8902, Japan*

⁷*Office of Space Applications, Japan Aerospace Exploration Agency,
Tsukuba, Ibaraki 305-8505, Japan*

(Received 0 0; accepted 0 0)

Abstract

We report preliminary results of AKARI observations of two globular clusters, NGC104 and NGC362. Imaging data covering areas of about 10×10 arcmin² centered on the two clusters have been obtained with InfraRed Camera (IRC) at 2.4, 3.2, 4.1, 7.0, 9.0, 11.0, 15.0, 18.0 and 24.0 μ m. We used F_{11}/F_2 and F_{24}/F_7 flux ratios as diagnostics of circumstellar dust emission. Dust emissions are mainly detected from variable stars obviously on the asymptotic giant branch, but some variable stars that reside below the tip of the first-ascending giant branch also show dust emissions. We found eight red sources with F_{24}/F_7 ratio greater than unity in NGC362. Six out of the eight have no 2MASS counterparts. However, we found no such source in NGC104.

Key words: infrared:stars stars:AGB and post-AGB Galaxy:globular clusters:individual (NGC104, NGC362)

1. Introduction

In order to calibrate the geometric distortion of the InfraRed Camera (IRC; Onaka et al. 2007) onboard AKARI (Murakami et al. 2007), we observed two galactic globular clusters, namely NGC104 (= 47 Tuc) and NGC362 during the AKARI in-orbit performance verification phase. Four pointings were dedicated for these observations. Here, we will use these data to study the evolution of low-mass stars with an emphasis on mass loss from them.

Galactic globular clusters are the best test grounds for stellar evolution theories of low-mass stars, since we can reasonably assume that they are composed of a single stellar population – that is, their constituent stars were formed at the same time, in the same volume of space, and from the same cloud of gas. Understanding of the

evolution of low-mass stars is important because they may lose as much as $\sim 40\%$ of their initial mass during their life time (Wachter et al. 2002), and also, as they represent the majority of the stars in the Galaxy, their role in the galactic formation and evolution is not negligible (e.g., Schröder and Sedlmayr 2001).

The mass loss process, which dominates the evolution of the star itself, is still a poorly understood phenomenon. Many observations (e.g., Tanabé et al. 1997) showed that the phase of the highest mass loss rate is achieved during the last stage of the asymptotic giant branch (AGB) evolutionary phase. Although it is not a large scale, however, mass loss also occurs along the first-ascending giant branch (RGB). It should exert a greater effect on stellar evolution, especially for low mass stars, given that their residence time in the RGB is much longer than that in the AGB (Schröder and Cuntz 2005).

NGC104 and NGC362 are well suited for studying a mass loss history along the RGB and AGB, because of well populated RGB and AGB stars. AKARI/IRC can detect red giants well below the tip of the RGB in the two clusters. The basic parameters of NGC104 and NGC362 are listed in Table 1, and a short description of each cluster including introductions of previous work follows.

Table 1. The basic parameters of NGC104 and NGC362.

	NGC104	NGC362
DM [mag]*	13.50 ± 0.08^1	15.06^3
[Fe/H]	-0.66^2	-1.12^3
Age [Gyr]	11.2 ± 1.1^1	$8 \sim 9^3$

* Distance modulus.

References: ¹ Gratton et al. (2003), ² Carretta and Gratton (1997), ³ Gratton et al. (1997)

1.1. NGC104

NGC104 is the second brightest (after ω Cen) galactic globular cluster. To date, 42 long period variables have been found (Lebzelter & Wood 2005). Mid-IR surveys of this cluster have been done by using the ISOCAM (Cesarsky et al. 1996) on board the Infrared Space Observatory (ISO; Kessler et al. 1996) to study the evolution of dust mass loss along the RGB and AGB (e.g., Ramdani and Jorissen 2001, Origlia et al. 2002). Ramdani and Jorissen (2001) observed outer regions of NGC104, and Origlia et al. (2002) observed an area of about $5' \times 3'$ centered on the cluster core. The IRC's wide field of view ($10' \times 10'$) enables us to cover both the central and outer regions within a single observation.

1.2. NGC362

This cluster is also well studied. Along with NGC288 it forms one of the most famous "second parameter" couples. NGC362 and NGC288 have about the same metallicities (= "the first or main parameter"), but their horizontal-branch (HB) morphologies are different. NGC362 has a red HB morphology, while NGC288 has a blue one (e.g., Sandage and Wallerstein 1960, Bolte 1989, Green and Norris 1990). To explain the difference, there must be at least one "second parameter". There are many second parameter candidates, e.g., cluster age, mass loss along the RGB, helium abundance, rotation and deep helium mixing, dynamical interactions involving binaries and even planets, environmental effects in high-density environments, and so on (e.g., Vink and Cassisi 2002 and references therein), and its origin is still a controversy (e.g., Stetson et al. 1996). Mass loss episodes along the RGB may be an "inclusive" second parameter (Catelan et al. 2001), as they are derivative (i.e., determined by other parameters of the star). Origlia et al. (2002) also observed this cluster, finding three stars with mid-infrared excess.

2. Observations & Reductions

Imaging observations of NGC104 and NGC362 were obtained on 2006 May 1st (NGC104), and 6th and 7th (NGC362) UT with the IRC. The IRC03 AKARI IRC observing template (AOT03) was used, yielding imaging data at 2.4, 3.2, 4.1, 7.0, 9.0, 11.0, 15.0, 18.0 and 24.0 μm taken in at least 2 dithered positions.

Raw data were processed with the IRC imaging data pipeline, version 070104 (see IRC Data User's Manual Lorente et al. (2007) for details). The resultant IRC mosaic images have pixel sizes of $1''.46 \text{ pixel}^{-1}$, $2''.40 \text{ pixel}^{-1}$ and $2''.38 \text{ pixel}^{-1}$ for NIR (2.4, 3.2, and 4.1 μm), MIR-S (7.0, 9.0, and 11.0 μm) and MIR-L (15.0, 18.0 and 24.0 μm) channels of IRC, respectively, covering an area $\sim 100 \text{ arcmin}^2$ around the cores of NGC104 and NGC362 in each wavelength.

2.1. Photometry

To derive calibrated fluxes for each star, point spread function (PSF) fitting photometry was performed on the mosaiced images with the IRAF¹ package DAOPHOT. Photometry was done for each mosaiced image independently. This involved the following steps:

1. DAOFIND was used to find stars whose fluxes are at least 5σ above the background, where σ is the background noise estimated locally around stars.
2. Aperture photometry was performed on all of the stars found in step 1, using the task PHOT with aperture radii of 10.0 and 7.5 pixels for NIR and MIR-S/MIR-L images, respectively. We used the same aperture radii as had been used in the standard star flux calibration (Tanabé et al. in preparation), so the aperture corrections were not applied. The resultant astronomical data units were converted to the calibrated fluxes by using the IRC flux calibration constants version 070119.
3. Several stars with moderate flux (i.e., with a good signal-to-noise ratio and unsaturated) and without neighbors within 7 pixels were selected from the results of step 2. We found more than 5 such stars in each mosaiced image. The selected stars were used to construct a model PSF.
4. The PSF fit was adopted to all of the stars found in the mosaiced images using ALLSTAR to get their instrumental fluxes and their corresponding errors. To check the array-location-dependence, we ran ALLSTAR with an option that the PSF can be linearly variable over the images. With this test, we found that the PSF does not vary significantly over the array. Hence constant PSF is assumed over an image.
5. The resultant instrumental fluxes were shifted so that the instrumental fluxes of the stars selected in

¹ IRAF is distributed by the National Optical Astronomy Observatories, which are operated by the Association of Universities for Research in Astronomy, Inc., under cooperative agreement with the National Science Foundation.

step 3 match the calibrated fluxes calculated in step 2.

We do not deredden the measured fluxes, but we applied color corrections on the calibrated fluxes by assuming a black body with the effective temperature of 3500 K. The temperature change of ± 500 K yields 2.4% change in the correction factor in the $2.4 \mu\text{m}$ case, but less than 1.0% for the others. Therefore, any discussions followed are almost insensitive to the assumed reference black body temperature.

2.2. Cross-identification with 2MASS sources

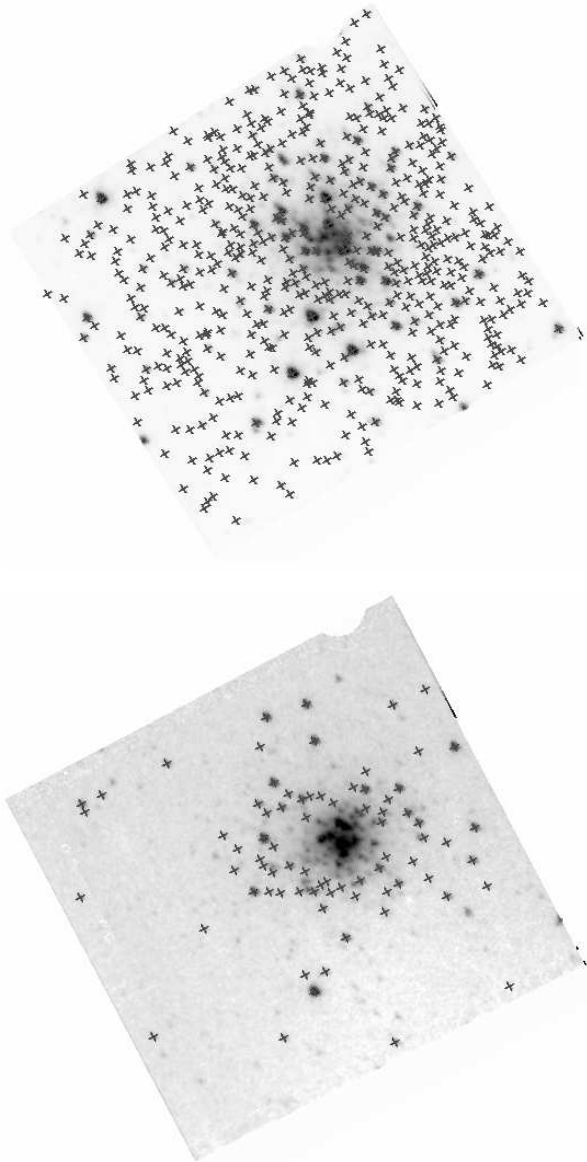


Fig. 1. AKARI IRC $11.0 \mu\text{m}$ image of NGC104 (top) and NGC362 (bottom). Crosses show IRC $11.0 \mu\text{m}$ sources with 2MASS counterpart. North is up, and east is to the left.

Cross-correlation of the IRC sources with 2MASS sources has been made in order to determine the astromet-

ric coordinates of detected sources in the mosaiced images of each wavelength. As the result, their coordinates were determined to the accuracy of about $2''0$ relative to the corresponding 2MASS sources. In Figure 1, we show the results of the cross-correlation between AKARI IRC $11.0 \mu\text{m}$ and 2MASS sources. The background images are IRC $11.0 \mu\text{m}$ images of NGC104 (top) and NGC362 (bottom). Crosses represent the IRC $11.0 \mu\text{m}$ sources with 2MASS counterparts within a radius of $1''0$.

After this cross-correlation, we inspected each source with $K_{2\text{MASS}} < 13.0$ mag by the eye to remove mis-identifications. Since we worked with the photometric data in high stellar density regions, we eliminated any IRC sources that were merged (we assumed that any IRC sources that have neighbor(s) within a half width at half maximum of the PSF of each wavelength as merged) with a brighter star, because they would introduce elements of confusion into the following discussions.

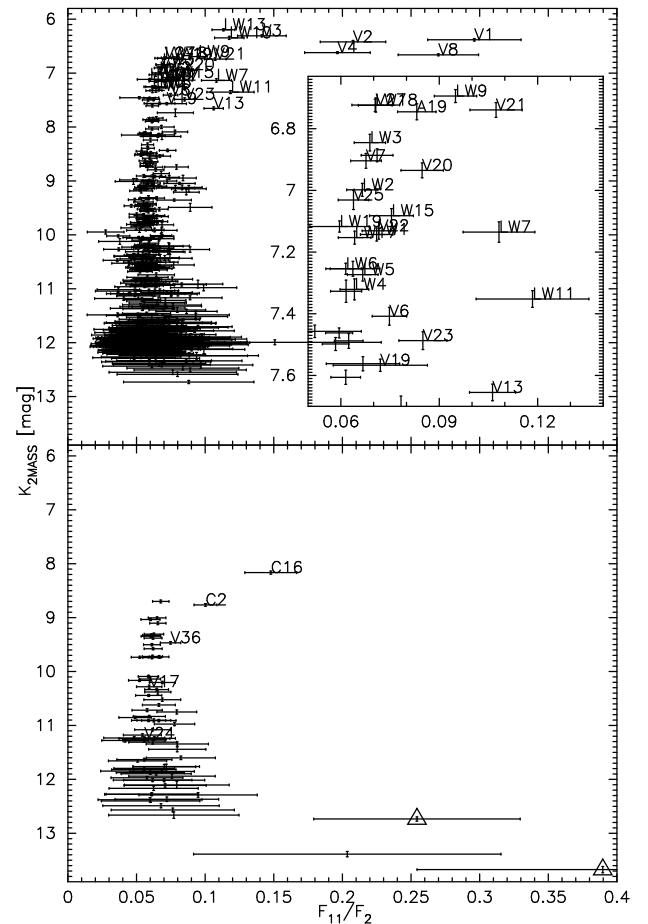


Fig. 2. The F_{11}/F_2 vs K_s diagram for sample stars with the variable stars identified. We use the nomenclature of Lebzelter & Wood (2005) for NGC104, and Szekély et al. (2007) for NGC362, except for two stars C2 and C16 (see text). The F_2 flux densities were calculated from K_s magnitude by adopting the zero-magnitude flux of 666.7 Jy (Cohen et al. 2003). See section 3.3 for the two triangles in NGC362. Closeup around the crowded part is shown in the inset.

3. Results & Discussion

3.1. Infrared excess of cluster stars

Ramdani and Jorissen (2001) showed that the ratio of the ISO 11.5 μm to DENIS K_s 2 μm flux density is a good indicator of dust mass loss. Therefore, we made a IRC 11.0 μm to 2MASS K_s flux density ratio (F_{11}/F_2) vs $K_{2\text{MASS}}$ diagram of our sample to see which stars show circumstellar dust emission. Hereafter, we denote 2MASS K_s as K_s unless otherwise described. The top panel of Figure 2 is plotted for NGC104, and the bottom for NGC362. The K_s fluxes (F_2) were calculated from K_s magnitudes by adopting the zero-magnitude flux of 666.7 Jy (Cohen et al. 2003). We did not apply reddening correction on 2MASS nor IRC fluxes. To get a basic idea, we calculated the F_{11}/F_2 ratio expected for a dust-free stellar atmosphere by using ATLAS9 (Kurucz 1993; Sbordone et al. 2004; Sbordone 2005). It came out that a star of $T_{\text{eff}} = 3500$ K, $\log g = 1.5$, $v_{\text{turb}} = 2.0$ km/s, and $[\text{Fe}/\text{H}] = -1.0$ would have F_{11}/F_2 ratio of about 0.065, showing that the F_{11}/F_2 ratios for most of the stars in NGC104 and NGC362 are consistent with the value predicted for dust-free photospheres. Further experiments with ATLAS9 showed that metallicity has a negligible impact on the F_{11}/F_2 ratio.

As it has been suggested by several authors (e.g., Vassiliadis and Wood 1993), stellar pulsations play a key role to trigger dust mass loss. The present results also show that all of the bright red giants with F_{11} excess ($F_{11}/F_2 \geq 0.1$) are indeed variables. Throughout this paper, we use the nomenclature of Lebzelter & Wood (2005) for variable stars in NGC104, and of Szekély et al. (2007) for ones in NGC362, except for C2 and C16. We have to note that the variable stars C2 and C16 in NGC362 are not listed in Szekély et al. (2007), but they are identical to V2 and V16 listed in Clement et al. (2001). It is confirmed by a near-infrared monitoring survey conducted by one of us (N. Matsunaga) that C2 is a semi-regular variable with a pulsation period of about 90 days, and also that C16 is a Mira-like variable with a pulsation period of about 135 days (Sawyer 1931; Matsunaga 2007).

Two sources in NGC104 with $K_s \sim 12.0$ and one source in NGC362 with $K_s \sim 13.4$ may have F_{11}/F_2 ratios greater than 0.1, but their photometric errors prevent us from regarding them as sources with infrared excess. Flux determinations of these three stars need further examination because they have much larger error bars than other stars at similar magnitudes. Put it all together, we found eleven stars (V1, V2, V3, V4, V8, V13, V21, LW7, LW10, LW11, and LW13) and two stars (C2 and C16) with infrared excess ($F_{11}/F_2 \geq 0.1$) in our observed fields of NGC104 and NGC362, respectively.

3.2. Infrared excess from RGB stars in NGC104?

Figure 2 also illustrates that a few variable stars below the tip of the first red giant branch (TRGB) in NGC104 do exhibit infrared excess. The TRGB occurs at $K = 6.75 \sim 7.1$ mag in NGC104 (Ferraro et al. 2000; Lebzelter & Wood 2005), and specifically, V13, LW7, and LW11 show

large ($F_{11}/F_2 \geq 0.1$) infrared excess although they reside below the TRGB. These three stars have similar pulsation periods of about 40 days and also similar ($J - K$) colors of about 1.0 (Lebzelter & Wood 2005). The period and ($J - K$) color are both being typical of variable stars below the TRGB found in the Large and Small Magellanic Clouds (Kiss and Bedding 2003; Ita et al. 2004a; Ita et al. 2004b). As in Ita et al. (2002), stars below the TRGB could be either on the AGB or the RGB, but a substantial fraction could be RGB stars. The definite identification of the evolutionary stage of these stars is difficult based solely on the present data. We cannot rule out the possibility that they are thermally-pulsating AGB stars during the phase of quiescent helium burning, when stars are fainter by just over a magnitude (Marigo et al. 2003). Further observations of each star is definitely needed for detailed study.

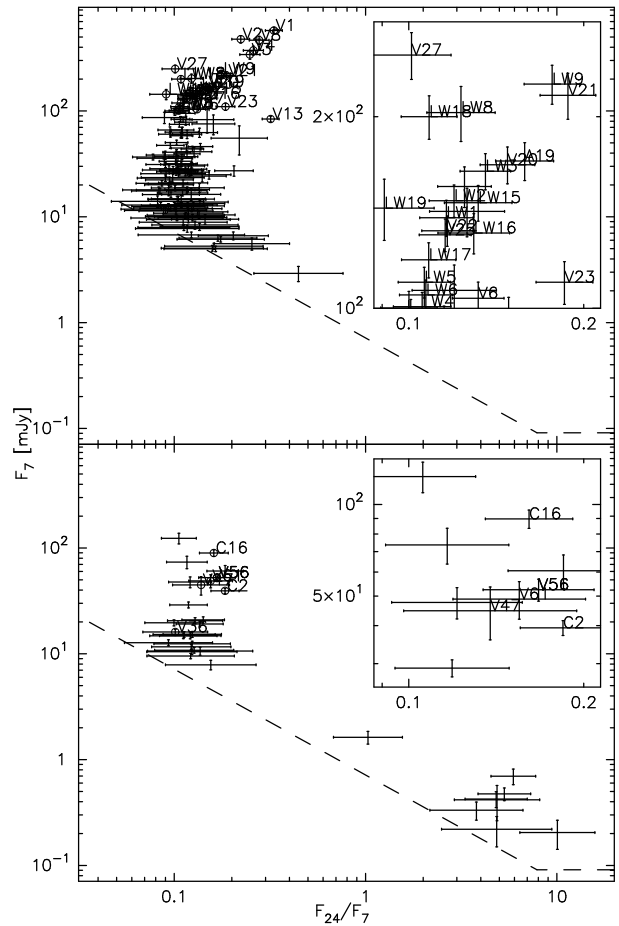


Fig. 3. The F_{24}/F_7 vs F_7 diagram for sample stars with the variable stars identified as in figure 2. The dashed lines shows 5σ sensitivity limit for AOT03 in one pointed observation, as given in Onaka et al. 2007. Note that fluxes are color-corrected, but not dereddened. Closeup around the crowded part is shown in the inset.

Interestingly, V13 in NGC104 has a F_{24}/F_7 ratio comparable to that of V1 (see the top panel of Figure 3), which has the longest pulsation period, largest pulsation ampli-

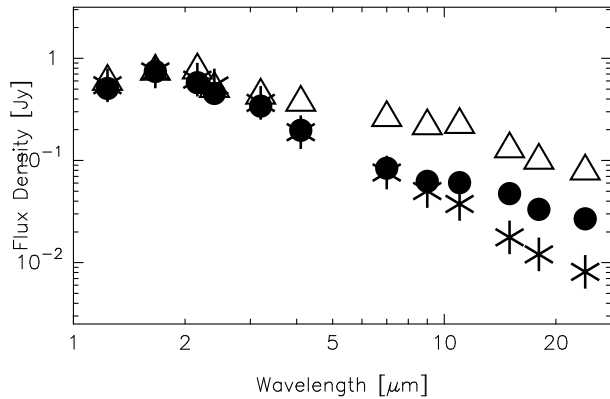


Fig. 4. The spectral energy distribution of V13 (filled circles), 2MASS 00234761–7202498 (asterisks), and V1 (triangles) in NGC104. Note that the fluxes of 2MASS 00234761–7202498 and V1 are scaled so that the H -band flux densities of them are matched to that of V13. Photometric errors are smaller than the size of the marks.

tude, and highest luminosity among all the members of NGC104, and shows the typical silicate dust feature in its mid-IR spectrum with a mass-loss rate of $\sim 10^{-6} M_{\odot} \text{yr}^{-1}$ (van Loon et al. 2006). We show the spectral energy distribution (SED) of V13 in Figure 4 using 2MASS JHK_s and all of the IRC fluxes. To emphasize the uniqueness of V13 compared to other normal red giants and also to genuine mass-losing AGB stars, the SED of a red giant, namely 2MASS 00234761-7202498 in NGC104 that has similar K_s magnitude and $(J - K_s)$ color ($K_s = 7.606$ mag, and $J - K_s = 1.081$ mag) as those of V13 ($K_s = 7.755$ mag, and $J - K_s = 1.089$ mag), and also V1 are included in the figure. For comparison, the fluxes of 2MASS 00234761-7202498 and V1 are multiplied by a factor of 1.022 and 0.410, respectively, that were calculated as the H -band flux densities of V13, 2MASS 00234761-7202498, and V1 are matched. We also calculated the absolute bolometric magnitude of V13 by fitting two black body curves with $T_{\text{eff}} = 3261$ K and $T_{\text{eff}} = 263$ K to the observed data. We obtained $M_{\text{bol}} \sim -3.11$ mag as a result, using the distance modulus of 13.5 mag for NGC104 (see Table 1). Lebzelter et al. (2006) took low-resolution mid-infrared (7.6–21.7 μm) spectra of V13 with the Spitzer telescope. They showed that V13 is devoid of a 9.7 μm emission band feature of amorphous silicate, but it has broad emission features at 11.5 μm (likely to be Al_2O_3), 13 μm (likely to be an Al–O stretching vibration), and 20 μm (no firm identification). Our results are consistent with theirs, showing that the infrared excess is detected at longward of 11.0 μm (Figure 4). Aluminium oxide features have been detected from low mass loss rate oxygen-rich AGB stars (Onaka et al. 1989; Kozasa and Sogawa 1997). Combined with the fact that the F_{11}/F_2 ratio of V13 is not so large, these results show that dust composition of V13 is different from those of usual mass losing AGB stars.

3.3. Very red sources in NGC362

Boyer et al. (2006) observed M15 with IRAC (Fazio et al. 2004) and MIPS (Rieke et al. 2004) onboard Spitzer Space Telescope (Werner et al. 2004). Their F_{24}/F_8 vs F_8 diagram revealed that there are at least 23 red sources in M15. They suggested that the red sources are mass-losing AGB or post-AGB candidates after consideration of their loose spatial distribution,

We use our 7.0 and 24.0 μm data to make the F_{24}/F_7 vs F_7 diagram, as shown in Figure 3. The top panel is for NGC104 and the bottom is for NGC362. It is seen that there are no sources with $F_{24}/F_7 \geq 1.0$ in NGC104, but there are eight red sources in NGC362. Six out of the eight have no 2MASS counterparts within a radius of $6''$. The other two sources with 2MASS counterparts have large F_{11}/F_2 ratios, as seen in Figure 2 (triangles). The spatial distribution of the eight sources are shown in Figure 5, indicating that they are distributed around the cluster, and are not biased to the cluster center.

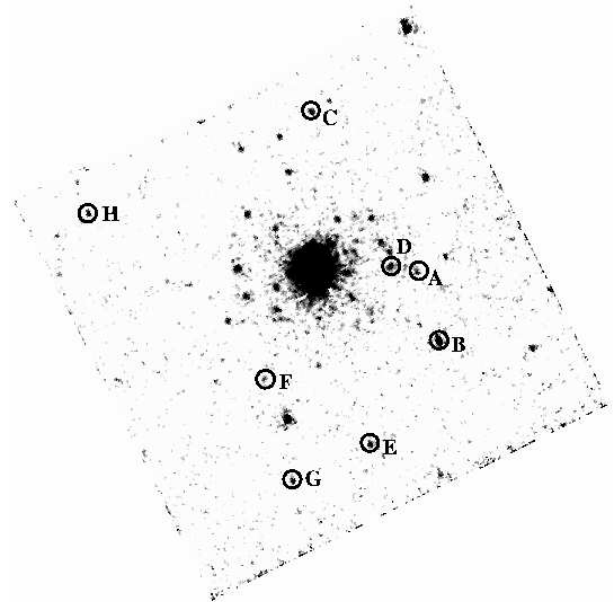


Fig. 5. AKARI IRC 24.0 μm image of NGC362 with eight red sources ($F_{24}/F_7 > 1.0$, see text) identified. their spectral energy distributions are shown in Figure 6. North is up, and east is to the left.

According to a model calculation (Pearson et al. in preparation), we can expect one or two galaxies in the IRC 100 arcmin² field of view down to the 5σ sensitivity limit of 24 μm . Then, there is little possibility that these sources are all background galaxies. Absence of red sources in NGC104 also suggests it unlikely that they are all galaxies. It is also unlikely that they are mass-losing AGB stars in NGC362, because their F_7 flux densities are too faint (Groenewegen 2006). Boyer et al. (2006) found similar objects in M15 by Spitzer observations and pointed out the possibility that they could be post-AGB stars. However, the fact that no clear counterparts have been seen at NIR wavelengths may be incompatible with

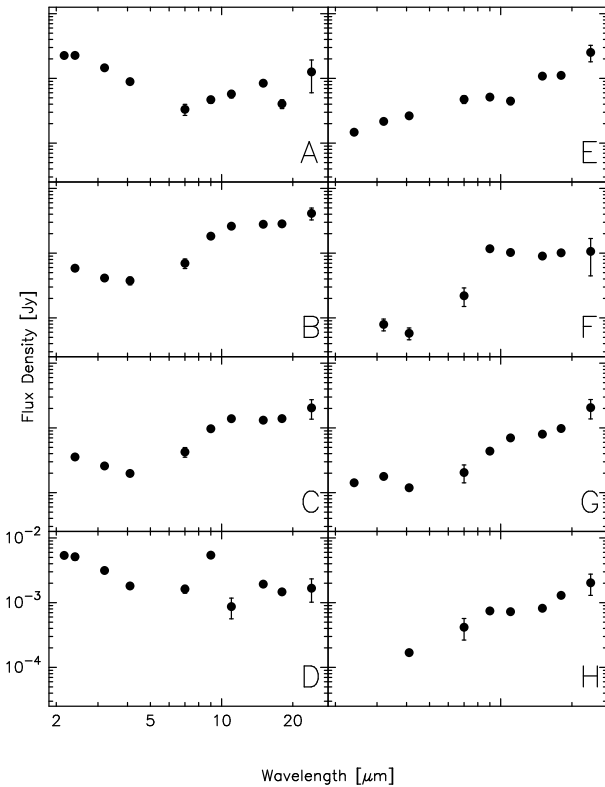


Fig. 6. Spectral energy distributions of the eight red sources in NGC362 showing K_s (if available) and all of the AKARI/IRC data. Note that some stars were not detected even in the NIR channel of IRC. The scales on the x- and y-axis are the same for each panel. The labels are as in Figure 5.

the post-AGB identification. NGC362 lies near the Small Magellanic Cloud in projection, therefore they might be bright high-mass-losing AGB stars in the SMC. However, such stars should be very rare, and we would not expect to detect eight of such stars in a 100 arcmin^2 field. We show the spectral energy distributions of the eight sources in Figure 6. It can be seen that infrared excess is detected not only at $24.0 \mu\text{m}$ but also at 15.0 and $18.0 \mu\text{m}$. Therefore it is likely that the excess is continuum emission and that the contribution from line emission such as $[\text{O IV}] 26 \mu\text{m}$ is insignificant. Some spectra show peculiar features, but the presence of the excess seems to be secure (based on the multi-band photometry). To identify the eight red sources and also to confirm the photometric results, infrared spectroscopic observations with AKARI and/or Spitzer would be needed.

4. Summary

We presented the first AKARI/IRC imaging data of NGC104 and NGC362. We found that stars with large F_{11}/F_2 ratio are all variables, confirming the close link between mass loss and stellar pulsation. We detected eight sources with large F_{24}/F_7 ratio in NGC362, but no such sources were present in NGC104. We also showed that V13 in NGC104 has interesting features, as being a pos-

sible RGB candidate with infrared excess.

Acknowledgements

We thank the referee for his/her useful comments which helped us improve this paper. We would like to thank Chris Pearson for making his latest galaxy count model calculations available in advance of publication. We also thank Michael Feast for helpful comments on the first version of the manuscript. AKARI is a JAXA project with the participation of ESA. This work is supported by the Grant-in-Aid for Encouragement of Young Scientists (B) No. 17740120 from the Ministry of Education, Culture, Sports, Science and Technology of Japan. This publication makes use of data products from the Two Micron All Sky Survey, which is a joint project of the University of Massachusetts and the Infrared Processing and Analysis Center, Caltech, funded by the National Aeronautics and Space Administration and the National Science Foundation.

References

- Bolte M. 1989, *AJ*, 97, 1688
- Boyer M.L, Woodward C.E., van Loon J.Th, et al. 2006, *AJ*, 132, 1415
- Carretta E., Gratton R.G. 1997, *A&AS*, 121, 95
- Catelan M., Bellazzini M., Landsman W.B., 2001, *AJ*, 122, 3171
- Cesarsky C., Abergel A., Agnese P., et al. 1996, *A&A*, 315, L32
- Clement C.M., Muzzin A., Dufton Q. 2001, *AJ*, 122, 2587
- Cohen M., Wheaton W. A., & Megeath S.T. 2003, *AJ*, 126, 1090
- Fazio G.G., Hora J.L., Allen L.E., et al. 2004, *ApJS*, 154, 10
- Ferraro F.R., Montegriffo P., Origlia L., et al. 2000, *AJ*, 119, 1282
- Gratton R.G., Fusi Pecci F., Carretta E., et al. 1997, *astro-ph/9707107*
- Gratton R.G., Bragaglia A., Carretta E., et al. 2003, *A&A*, 408, 529
- Green E.M., Norris J.E. 1990, *ApJ*, 353, L117
- Groenewegen M.A.T 2006, *A&A*, 448, 181
- Ita Y., Tanabè T., Matsunaga N., et al. 2002, *MNRAS*, 337, L31
- Ita Y., Tanabè T., Matsunaga N., et al. 2004a, *MNRAS*, 347, 720
- Ita Y., Tanabè T., Matsunaga N., et al. 2004b, *MNRAS*, 353, 705
- Kessler M.F., Steinz J.A., Anderegg M.E., et al. 1996, *A&A*, 315, L27
- Kiss L.L, Bedding T.R., 2003, *MNRAS*, 343, 79
- Kozasa T., Sogawa H., 1997, *Ap&SS*, 251, 165
- Kurucz R.L. 1993, *ATLAS9 Stellar Atmosphere Programs and 2 km/s grid*. Kurucz CD-ROM No. 13. Cambridge, Mass.: Smithsonian Astrophysical Observatory, 1993., 13
- Lebzelter T., Wood P.R. 2005, *A&A*, 441, 1117
- Lebzelter T., Posch T., Hinkle K., et al., 2006, *ApJ*, 653, L145
- Lorente R., Onaka T., Ita Y., et al., 2007, *AKARI IRC Data User's Manual ver. 1.1*, <http://www.ir.isas.jaxa.jp/AKARI/Observation/>
- Marigo P., Girardi L., Chiosi C., 2003, *A&A*, 403, 225

- Matsunaga N., 2007, Ph.D. thesis, University of Tokyo
Murakami H., et al., 2007, PASJ, submitted
Onaka T., De Jong T., Willems F.J., 1989, A&A, 218, 1690
Onaka T., et al., 2007, PASJ, submitted
Origlia L., Ferraro F.R., Pecci F.F., et al. 2002, ApJ, 571, 458
Ramdani A., Jorissen A. 2001, A&AS 372, 85
Rieke G.H., Young E.T., Engelbracht C.W., et al. 2004, ApJS, 154, 25
Sandage A., Wallerstein G. 1960, ApJ, 131, 598
Sawyer, H.B, 1931, Harvard College Observatory Circular, vol. 366, pp.1-36
Sbordone L., Bonifacio P., Castelli F. & Kurucz, R.L. 2004, Memorie della Societa Astronomica Italiana Supplement, 5, 93
Sbordone L. 2005, Memorie della Societa Astronomica Italiana Supplement, 8, 61
Schröder K.-P., Sedlmayr E. 2001, A&A, 366, 913
Schröder K.-P., Cuntz M. 2005, ApJ, 630, L73
Stetson P.B., VandenBerg D.A. & Bolte M.J. 1996, PASP, 108, 560
Szekely P., Kiss L.L., Jackson R., et al. 2007, astro-ph/0611663
Tanabe T., Nishida S., Matsumoto S., et al. 1997, Natur, 385, 509
van Loon J.Th, McDonald M., Oliveira J.M., et al. 2006, A&A, 450, 339
Vassiliadis E., Wood P.R. 1993, ApJ, 413, 641
Vink J.S., Cassisi S., 2002, A&A, 392, 553
Wachter A., Schröder K.-P., Winters J.M., et al. 2002, A&A, 384, 452
Werner M.W., Roellig T.L., Low F.J., 2004, ApJS, 154, 1